International Journal of Heat and Mass Transfer 126 (2018) 1358–1375

Contents lists available at ScienceDirect

International Journal of Heat and Mass Transfer

journal homepage: www.elsevier.com/locate/ijhmt

Effects of Prandtl number on the forced convection heat transfer from a porous square cylinder

K. Anirudh, S. Dhinakaran *

The Centre for Fluid Dynamics, Discipline of Mechanical Engineering, Indian Institute of Technology Indore, Simrol, Indore 453 552, India

ARTICLE INFO

Article history:
Received 8 February 2018
Received in revised form 9 May 2018
Accepted 1 June 2018
Available online 26 July 2018

Keywords:
Prandtl number
Heat transfer
Darcy-Brinkman-Forchheimer model
OpenFOAM 5.0
Porous square cylinder

ABSTRACT

Combined influence of Prandtl number and Darcy number variations on heat transfer from a two-dimensional porous square cylinder, placed in an unconfined computational domain, is investigated numerically for $Pr = 0.71–100$. The porous cylinder is subjected to a steady cross-flow regime with Reynolds number and Darcy number varying between $Re = 1–40$ and $Da = 10^{-6} – 10^{-2}$. Numerical simulations are carried out by modifying the generic buoyantBoussinesqPimpleFoam solver of OpenFOAM 5.0 coupled with Darcy-Brinkman-Forchheimer model, with single domain approach. Significant augmentation in heat transfer rate from the porous cylinder is reported by varying *Pr*, *Re* and *Da*. Detailed insight on the mechanism behind this thermal enhancement is provided through isotherm contours, temperature profiles and local, surface averaged and mean Nusselt number plots. A brief description on the relation between jump phenomenon that occurs in flow characteristics for porous square cylinder and heat transfer results is also given. An insight on the inclusion of Forchheimer source term in the steady flow regime is provided. Finally, correlations are provided for the mean Nusselt number for a few values of *Pr* and *Da* in terms of *Re*. Optimistically, scholars and engineers working on heat transfer increment through usage of porous material or intending to numerically model porous media theory will benefit from the information presented in this article.

1. Introduction

Flow and heat transfer from porous bluff bodies have been interesting researchers over the past few decades due to their practical and computational significance. Such phenomena can be seen to occur in idealisation of the flow in electronic devices using porous heat sinks, microcarriers or scaffolds in a bioreactor, liquid-solid reactors with settling of flocs of material, control rod arrangement in a nuclear reactor core and filters used in pharmaceutical and chemical industries. The computational significance of these occurrences can be appreciated when numerical simulations across significant number of identical bodies have to be performed. A suitable assumption of relevant porous bluff body shape transforms the problem, providing significant computational economy and simplicity in terms of numerical modelling.

It is well-known that a porous material provides augmentation in heat transfer rate due its internal tortuous paths, which provide surplus surface area for better thermal dissipation. Additional efforts can be further put into for increasing heat exchange by using a working fluid with higher thermal conductivity i.e. higher Prandtl number, *Pr*. A broad spectrum of literature on thermal enhancement concentrates on this topic i.e., effects of different working fluids, with various Prandtl numbers, on augmentation in heat transfer. Dhiman et al. [1] studied the confined flow across a solid square cylinder for a wide range of *Pr* ($Pr = 0.71–4000$) in the steady flow regime (Reynolds number, $Re = 1–45$) at different blockage ratios (β = 1/8, 1/6 and 1/4). They performed the numerical simulations for two different thermal boundary condition i.e., constant wall temperature (CWT) and constant heat flux (CHF). Speaking broadly, the CHF boundary condition generally yields higher values of mean Nusselt number, Nu_M compared to CWT condition under otherwise similar conditions of β, *Re* and *Pr*. Moreover, this difference further increases with increasing *Re* and *Pr* values. The numerical results of their study yield that the average Nusselt number monotonically increases with *Re* and *Pr*. In another study by the authors [2], for the same setup with an unconfined computational domain, it was observed that local Nusselt number at each corner of the square cylinder increases proportionally with *Re* and *Pr*. The average Nusselt number was reported to be maximum at front surface of the cylinder, followed by top and bottom and least at the rear face. Bharti et al. [3] performed numerical computations to investigate flow and heat transfer from an unconfined circular cylinder at $Pr = 0.7–400$ and $Re = 10–45$. They too obtained a

* Corresponding author.
E-mail address: ssdhinakar@gmail.com (S. Dhinakaran).

https://doi.org/10.1016/j.ijheatmasstransfer.2018.06.003
0017-9310/

Nomenclature

$\bar{s}$	velocity of fluid in porous region, $(\mathrm{m\,s^{-1}})$
C_D	coefficient of drag, $Fd/(0.5\cdot\rho\cdot A\cdot U_\infty^2)$
D	height of cylinder (m)
d	diameter of the spherical particle of packed bed (m)
Da	Darcy number, κ/D^2
E	enhancement ratio
F	inertial factor, $(1.75/\sqrt{150})\cdot(1/\epsilon^{1.5})$
Fd	drag force acting on the porous cylinder (N)
k	thermal conductivity of the material $\mathrm{W/(m\,K)}$
L_D	distance between rear face of the cylinder and the outflow boundary (m)

Greek

α	thermal diffusivity $(\mathrm{m^2\,s^{-1}})$
Δ	largest grid size (m)
δ	smallest grid size (m)
ϵ	porosity
κ	permeability of the material $(\mathrm{m^2})$
μ	dynamic viscosity $(\mathrm{kg\,m^1\,s^1})$

Subscript

0	inlet value
∞	far field value
B	bottom face of the porous square cylinder
e	effective value
F	front face of the porous square cylinder
Nu	Nusselt number, $-R_k(\partial\theta)/(\partial n)$
P	dimensionless pressure, $p/(U_\infty^2)$
p	kinematic pressure of the fluid, $(\mathrm{m^2\,s^{-2}})$
Pr	Prandtl number, ν/α
R_k	thermal conductivity ratio, k_e/k_f
Re	Reynolds number, $U_\infty\cdot D/\nu$
T	dimensional temperature, $^\circ K$
t	dimensional time (s)
U,V	non-dimensional x,y – component of velocity, u/U_∞, v/U_∞
u,v	x,y – component of velocity $(m\cdot s^{-1})$
X,Y	non-dimensional horizontal, vertical distance, $x/D, y/D$
x,y	horizontal, vertical distance (m)
ν	kinematic viscosity $(\mathrm{m^2\,s^{-1}})$
ρ	density $(\mathrm{kg\,m^{-3}})$
τ	non-dimensional time, $t\cdot U_\infty/D$
θ	non-dimensional temperature $(T-T_\infty)/(T_D-T_\infty)$
f	value for fluid region
p	particle
R	rear face of the porous square cylinder
T	top face of the porous square cylinder
W	porous surface

monotonous rise in thermal dissipation from the heated cylinder after increasing Reynolds and Prandtl number. Further, in the unsteady cross flow regime ($Re = 60$—160), Sahu et al. [4] numerically studied heat transfer from a heated square cylinder in the 2Dunconfined computational domain at $Pr = 0.7$—50. Upon increasing Re and Pr, due to thinning of thermal boundary layer across the cylinder surfaces, they observed the local and surface Nusselt number at all faces of cylinder increase. However, at higher values of Re and Pr, they noticed the average Nusselt number at the rear face of the cylinder to exceed that of the top and bottom surface of the cylinder. Sarkar et al. [5] revealed the flow across a heated circular cylinder at $Re = 80$—180 and $Pr = 0.7$—100 in a numerical attempt using FEM. It is clear from their graphical representation of results that isotherms become steeper around the cylinder with increasing Pr and are incarcerate to a smaller region. As Reynolds number is increased, they cling more towards the near-wake region. They too suggested that Nusselt number indeed depends positively on Re and Pr, however, the dependence is more on Re compared to Pr. More recently, Kumar and Dhiman [6] simulated forced convection heat transfer from a square obstacle in the neighbourhood of a wall at $Re = 1$—$150, Pr = 10$—100 and gap ratios, $G = 0.25$—1. A maximum rise of approximately 1332% in heat transfer at Re = 150, Pr = 100 and G = 0.25 against analogous values at Re = 1. Other works on circular cylinder by Chen et al. [7] and Ajith Kumar et al. [8] suggest similar outcomes as the literature above on the effects of Prandtl number on heat transfer augmentation.

A wide range of literature is available on the subject matter for other bluff body shapes. Following is a review on selected works regarding forced convection heat transfer discussing effects of Prandtl number variation. Aboueian-Jahromi et al. [9] performed numerical simulations to study the influence of blockage ratio and Prandtl number on flow and heat transfer of Newtonian fluids across a diamond-shaped solid square cylinder for a wide range of Pr (Pr = 0.7–100) and three different β = 1/8, 1/6 and 1/4 in the steady cross flow regime. They suggest that at low Re and Pr, decreasing blockage ratio is an economical way of increasing heat transfer. For larger Re and Pr, Nusselt number is found to be in direct proportion with blockage ratio. Chandra and Chhabra [10] studied heat transfer from a semi-circular cylinder placed centrally in an unconfined computational domain at $Re = 0.01$—39.5 and $Pr = 0.71$—100. Apart from the usual observation of augmentation in heat transfer with Pr, they reported that maximum heat transfer occurs from the front curved surface and not from the rear flat surface. Further, Gode et al. [11] studied momentum and heat transfer characteristics of a 2D incompressible steady flow across a semi-circular cylinder with its base parallel to the flow. They also, have found stronger dependency of Nu_M on Re, compared to Pr. Recently, Kumar et al. [12] simulated confined ($\beta = 25\%$) flow of a Newtonian constant-property fluid across a semi-circular cylinder in the unsteady flow regime ($Re = 50$—200) at $Pr = 0.7, 10$ and 100. Unlike the common belief, they reveal that average Nusselt increases somewhat with Re and substantially with Pr for the entire range of Re and Pr considered. Ratio of Nu values belonging to $Pr = 100$ and those belonging to $Pr = 0.7$ range from 6.3 to 6.5. For unsteady forced convection heat transfer around a long equilateral triangular cylinder in an unconfined medium, Chatterjee and Mondal [13] carried out numerical simulations using air, water and engine oil as working fluid. They concluded that the overall flow patterns does not depend on Pr, however, isotherms vary significantly.

Contrary to the well-established concept that heat transfer augments with Pr, Dey and Das [14] state that during the transition of shape of heated square to circular cylinder, at various corner radii, heat transfer rate declines at higher Pr. Maximum enhancement in heat transfer of 14% was found at $Pr = 1$ and $r = 0.51$. This inference was drawn from two different numerical attempts using finite volume method [14] and artificial neural network [15], conducted for $Re = 80$—180 and the other for $Re = 100$ at $Pr = 0.01$—1000 and corner radii, $r = 0.5$—0.71, respectively. They reported a stronger dependence of Nusselt number on Prandtl number compared to Reynolds number.

It is a well established fact that at lower values of Darcy number the porous bluff body behaves like its solid counterpart. This

characteristic holds true for all momentum and heat transfer characteristics. However, at higher values of permeability, as the fluid flows more through the heated cylinder, the thermal transfer effect increases and the same has been reported by Wu and Wang [16]. They simulated convective heat transfer numerically from a porous square cylinder placed in a channel and heated at the bottom face for $Re = 100—700$, porosity, $\epsilon = 0.4—0.8$ and $Da = 10^{-6}—10^{-2}$. Negligible influence of porosity was found on the Nusselt number values in comparison to permeability. At higher values of *Da*, as more fluid enters the heated cylinder, more heat is carried away from it. Accordingly, a direct proportion between Nusselt number, Darcy number and Reynolds number was reported by the authors. Further, the authors [17] extended the study in the unsteady flow regime ($Re = 50—250$) for different channel-to-cylinder height ratios viz., 10%, 30% and 50%. Nusselt number value was observed to augment with decreasing cylinder-to-channel height ratio, alongwith increasing Darcy number. A maximum enhancement in Nu_M of 108.4% at $Da = 10^{-2}$ and $Re = 40$ was reported by Dhinakaran and Ponmozhi [18]. They carried out numerical computations to study unconfined flow and heat transfer from a porous square cylinder subjected a uniform steady cross-flow ($Re = 1—40$). They also reported that Nusselt number stays higher for front surface, followed by top and bottom and least at rear face of the cylinder. The difference in *Nu* values between these faces further widens at higher *Re* and *Da* values.

Above literature review dictates that the influence of Prandtl number on heat transfer augmentation has been well-studied for solid bluff bodies of various shapes, under different operating conditions. However, a detailed study on the same is missing for the case of porous bluff body, particularly for porous square cylinder. The present study focuses on effects of different working fluids on the thermal behaviour of a porous square cylinder. The current numerical attempt can facilitate the engineers interested in application of finite volume method to study the effects of different coolants circulated through micro porous heat sinks for thermal management of high power LEDs (shown in Fig. 1). The coolant is pumped through the porous heat sink, mostly at a uniform rate and hence, the present study focuses on forced convection heat transfer from a porous square cylinder subjected to uniform steady flow. Therefore, the Reynolds number is varied in the range of $1 \leqslant Re \leqslant 40$. It is assumed that after reaching steady-state the porous block would be heated in a uniform fashion, owing to which an unconfined flow across uniformly heated porous cylinder is considered here. This is because the manuscript primarily intends to critique on the effect of *Pr* on thermal boundary layer across porous surface and the influence of permeability on it, which inturn affects the thermal performance of the body. Representative fluids for the wide range of Prandtl number taken into account are air ($Pr = 0.71$), mixtures like Water-Potassium Formate, Water - Ethanol and Water - Methanol ($Pr = 1—10$) and different concentrations of Ethylene Glycol ($Pr = 10—100$). Further, in order to study wide levels of permeability i.e., from solid-like to through flow conditions, Darcy number is varied in the range of $10^{-6} \leqslant Re \leqslant 10^{-2}$.

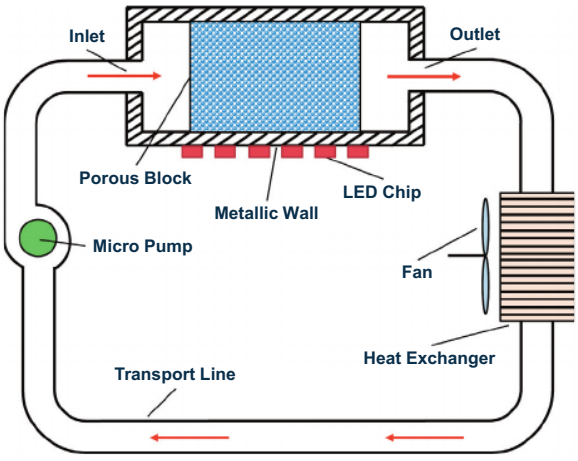

Fig. 1. Schematic diagram of porous micro heat sink system. Different coolants (various *Pr*) are pumped through the porous block mounted on heated electronic components for better thermal management. This figure is just a representative of possible application on numerical method advocated in this research paper. It is not a direct applicaiton of the present study.

2. Mathematical formulation

2.1. Problem description

A pictorial representation of problem under study is shown in Fig. 2(a). A fixed uniformly heated two-dimensional porous square cylinder of size '*D*', subjected to a cross flow with uniform free stream velocity (U_∞), is placed in an unconfined computational domain. The cylinder is maintained at a constant temperature 'T_W', higher than the ambient temperature 'T_∞', such that the porous cylinder exchanges heat with the surrounding fluid. Artificial boundaries are placed sufficiently far away from the heated body so as to make the problem computationally feasible.

2.2. Governing equations

With the above mentioned assumptions, the flow and heat transfer in clear fluid region is modelled by Navier-Stokes equation, given as,

Continuity equation:

$$\frac{\partial u}{\partial x} + \frac{\partial v}{\partial y} = 0, \tag{1}$$

Momentum equations:

$$\rho\left(\frac{\partial u}{\partial t} + u\frac{\partial u}{\partial x} + v\frac{\partial u}{\partial y}\right) = -\frac{\partial p}{\partial x} + \mu\left(\frac{\partial^2 u}{\partial x^2} + \frac{\partial^2 u}{\partial y^2}\right), \tag{2}$$

$$\rho\left(\frac{\partial v}{\partial t} + u\frac{\partial v}{\partial x} + v\frac{\partial v}{\partial y}\right) = -\frac{\partial p}{\partial y} + \mu\left(\frac{\partial^2 v}{\partial x^2} + \frac{\partial^2 v}{\partial y^2}\right), \text{and,} \tag{3}$$

Energy equation:

$$\frac{\partial T}{\partial t} + \left(u\frac{\partial T}{\partial x} + v\frac{\partial T}{\partial y}\right) = \alpha\left(\frac{\partial^2 T}{\partial x^2} + \frac{\partial^2 T}{\partial y^2}\right). \tag{4}$$

In the above equation, u and v represent x and y components of dimensional velocity, while p and T stand for dimensional pressure and temperature. The density, effective viscosity and thermal diffusivity are indicated by ρ, μ and α, respectively. Modifications in the above governing equations need to be done for modelling the flow and heat transfer in porous region. In the absence of porous media, the flow is known to occur with an artificial velocity referred to as superficial velocity. The physical or actual velocity may vary with location inside the complex porous region and it is hard to determine, while superficial velocity is relied on because it is readily known and is unambiguous. Presence of porous medium would obviously reduce the area available for superficial flow through the pores, causing the velocity to be higher

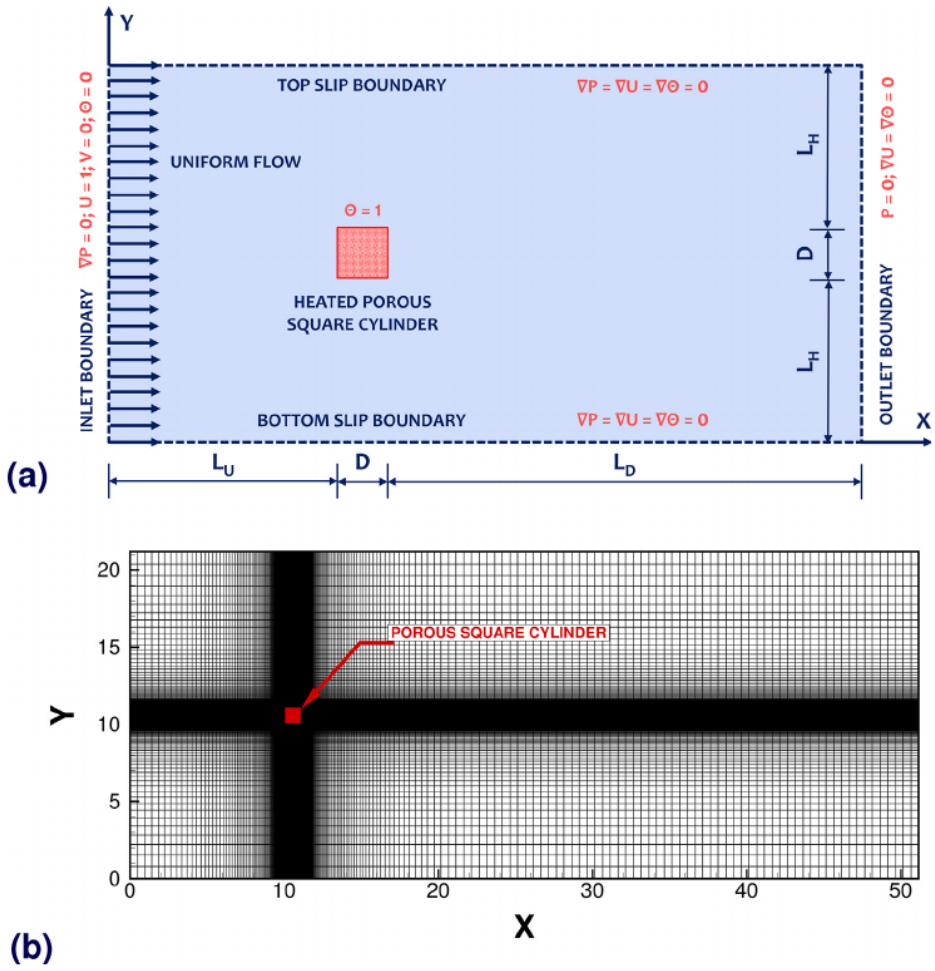

Fig. 2. (a) Schematic of the computational set-up for the heat transfer from a porous square cylinder, along with boundary conditions and (b) non-uniform mesh distribution in the computational domain that has been used for the numerical calculations.

than rest of the domain. Entity that relates the physical velocity in the porous region and the superficial velocity outside is porosity (ϵ), which is equal to the volume fraction of voids present in the medium. Therefore, the physical velocity is related to the superficial velocity as $\bar{s} = v/\epsilon$ and this introduces the '$1/\epsilon$' term next to velocity terms in the transport equation [19]. Additionally, source terms are introduced in the momentum equation for modelling the flow in porous region viz., Darcy and Forchheimer terms. Darcy term takes into account the existence of general porous resistance in the flow, while Brinkman coefficient (advection term along with porosity) brings into the viscous resistance offered by porous zone to the fluid flow. Forchheimer term, the second source term, looks after the inertial resistance offered by the porous media at higher *Re*. The resultant Darcy-Brinkman-Forchheimer extended model is the most applied numerical approach when it comes to flow through porous media [18]. However, as the validity of Forchheimer term in steady flow regime is under scrutiny, a section explaining its validity in the steady flow regime has been commented on in Section 5.6. The governing equations [16] solved in the current numerical computations in porous region are given as,

Continuity equation:

$$\frac{\partial u}{\partial x} + \frac{\partial v}{\partial y} = 0, \tag{5}$$

Momentum equations:

$$\rho\left(\frac{1}{\epsilon}\frac{\partial u}{\partial t} + \frac{u}{\epsilon^2}\frac{\partial u}{\partial x} + \frac{v}{\epsilon^2}\frac{\partial u}{\partial y}\right) = -\frac{\partial p}{\partial x} + \frac{\mu_e}{\epsilon}\left(\frac{\partial^2 u}{\partial x^2} + \frac{\partial^2 u}{\partial y^2}\right) - \frac{\mu}{\kappa}u - \frac{\rho F}{\sqrt{\kappa}}|\vec{V}|u, \tag{6}$$

$$\rho\left(\frac{1}{\epsilon}\frac{\partial v}{\partial t} + \frac{v}{\epsilon^2}\frac{\partial v}{\partial x} + \frac{v}{\epsilon^2}\frac{\partial v}{\partial y}\right) = -\frac{\partial p}{\partial y} + \frac{\mu_e}{\epsilon}\left(\frac{\partial^2 v}{\partial x^2} + \frac{\partial^2 v}{\partial y^2}\right) - \frac{\mu}{\kappa}v - \frac{\rho F}{\sqrt{\kappa}}|\vec{V}|v, \quad \text{and,} \tag{7}$$

Energy equation:

$$\frac{\partial T}{\partial t} + \left(\frac{u}{\epsilon}\frac{\partial T}{\partial x} + \frac{v}{\epsilon}\frac{\partial T}{\partial y}\right) = \alpha\left(\frac{\partial^2 T}{\partial x^2} + \frac{\partial^2 T}{\partial y^2}\right). \tag{8}$$

In the above equations, $|\vec{V}| = \sqrt{u^2 + v^2}$ is the resultant velocity and $F = \frac{1.75}{\sqrt{150}} \cdot \frac{1}{\epsilon^{1.5}}$ is the inertial factor [18]. Also, κ is permeability of the porous medium and μ_e is ratio of the viscosities of porous and fluid region.

2.3. Non-dimensionalisation of results

Since, using non-dimensional variables in OpenFOAM 5.0 is quite cumbersome, non-dimensionalisation of the output variables is done post-simulation, by using the following characteristic scales

$$X=\frac{x}{D},\quad Y=\frac{y}{D},\quad \tau=\frac{tU_\infty}{D},\quad P=\frac{p}{\rho U_\infty^2},\quad U=\frac{u}{U_\infty},$$
$$V=\frac{v}{U_\infty}\ \text{and}\ \theta=\frac{T-T_\infty}{T_W-T_\infty}. \tag{9}$$

Height of the cylinder and temperature of the porous cylinder surface are indicated by D and T_W, respectively. Also, U_∞ and T_∞ represent far-field velocity and temperature. Non-dimensional scales for x-distance, y-distance, time, pressure, x-velocity, y-velocity and temperature are denoted by X, Y, τ, P, U, V and θ, respectively.

2.4. Boundary conditions

As shown in Fig. 2(a), a uniform horizontal flow at ambient temperature is fed at the inlet of the domain i.e. $U=1, V=0,\ \nabla P = 0$, and $\theta=0$. At outlet of the domain, a zero-Gradient boundary condition for velocity and temperature terms is imposed i.e., $\nabla U=0$ and $\nabla\theta=0$. The absolute pressure at the outlet is kept zero, $P=0$. At the top and bottom boundary of the computational domain, slip boundary condition for velocity is applied and the pressure and temperature gradients are kept to be zero throughout. A constant temperature thermal boundary condition is imposed on the cylinder surface and it is always maintained at a higher temperature than the surrounding fluid i.e., $\theta=1$.

2.5. Relating porosity and permeability

The heated permeable cylinder in the current simulations is approximated to be made up of a packed bed of spherical particles. Number of these beads, their size, void between them and their connectivity decide the porosity and permeability of the medium and usually, during flow through porous media, they both are varied independently. While these parameters change, particle diameter (d_p) and/or number of particles in the medium vary, which changes the topography of entire medium during a simulation. Hence, for the sake of uniformity, non-dimensional size of the spherical particles comprising the medium is kept uniform throughout all computations to '$d_p/D=0.01$'. The porosity and permeability terms are linked together through the Carman-Kozeny relation [20], which is written as

$$Da=\frac{1}{180}\frac{\epsilon^3}{(1-\epsilon)^2}\left(\frac{d_p}{D}\right)^2=5.56\times10^{-7}\cdot\frac{\epsilon^3}{(1-\epsilon)^2}. \tag{10}$$

3. Numerical Details

In the present study, numerical computations are performed based on finite volume method and the open-source tool OpenFOAM 5.0 [21] is used. The generic 'buoyantBoussinesqPimpleFoam' solver (based on the combination of SIMPLE and PISO algorithm) of OpenFOAM 5.0 is modified by applying Darcy-Forchheimer-Brinkman model to it. The buoyancy is set to 'zero', as the present case is of forced convection. This solver helps to adjust the Courant number to a higher value, inturn speeding up the simulations to achieve a stable solution due to under-relaxation. Gauss linear scheme is used to account for time derivative, gradient, divergence and Laplacian terms and a linear interpolation scheme is used for the collocated grid. Further, the PCG solver with DIC pre-conditioner is used for pressure term and the smoothsolver with symGaussSiedel smoother is used for evaluating the velocity and temperature terms. Although OpenFOAM 5.0 does not use an explicit Rhie-Chow correction, the generic correction for pressure terms is believed to be 'Rhie-Chow inspired' [22]. The residual criteria for pressure, velocity and temperature terms is set to 10^{-10}, no under-relaxation is applied and the nOuterCorrectors are set to 50, nCorrectors to 2 and NonOrthogonalCorrectors to 0.

4. Grid generation and code validation

Generic blockMesh tool of OpenFOAM 5.0 is used for the generation of structured non-uniform mesh in the computational domain, as shown in Fig. 2(b). The fluid-porous interface requires special attention as intricate flow and heat transfer phenomena occur in this region. Hence, a fine uniform mesh is used in the porous cylinder and region of $0.1D$ around the cylinder, with an element size of $\delta=0.008D$. A non-uniform mesh with simple grading further extends up to a distance of $10D$ around the porous cylinder, with maximum element size of $\Delta=0.5D$ in horizontal direction and $\Delta=0.8D$ in the vertical direction. At lower Re, since the thermal plume expands upstream of the front cylinder surface and this expansion is further provoked by higher permeability, a large upstream length is required. A uniform mesh with element size $\Delta=0.5D$ then extends beyond this non-uniform mesh in the horizontal direction through the entire downstream length (L_D). A grid sensitivity analysis is carried out at $Re=40, Pr=100$ and $Da=10^{-6}$, to check the dependence of flow parameter, drag coefficient and thermal parameter, mean Nusselt number, on the grid size and downstream length. The sensitivity analysis is carried out at extremities of the parameter ranges considered in the study. At $Da=10^{-6}$, the viscous and inertial resistances introduced through Darcy-Brinkman-Forchheimer model is higher in comparison to $Da=10^{-2}$. Hence, various grids are tested at lower value of permeability, $Da=10^{-6}$. In this analysis, numerous test simulations were run learning about the optimal grid size for three different downstream lengths viz., L_D = $30D$, $40D$, and $50D$. Since, the study deals with higher Pr fluids, the isotherm at higher Da extends to the outer flow boundary. Owing to this fact, a longer downstream length is chosen. The current solver is tested for four different grids of $X\times Y$ sizes viz., 250×148 (Grid A), 334×206 (Grid B), 371×259 (Grid C) and 476×356 (Grid D). Table 1 gives the details of the grid-independence study for different downstream lengths. After a close observation of the given values, keeping both accuracy and computational economy into mind, Grid C with L_D = 40 is chosen (marked with $*$ in Table 1). Width of the uniform mesh around the cylinder influences the thermal results, hence, different widths are analysed and it is found that $0.1D$ gives minimum error (around 2%) and is optimum in terms of computational economy. Also, to avoid influence of domain height on the final results, three different domain heights viz, $21D$, $25D$ and

Table 1
Grid sensitivity and downstream length dependence test on coefficient of drag, C_D and mean Nusselt number, Nu_M at Prandtl number, $Pr=100$, Darcy number, $Da=10^{-6}$ and Reynolds number, $Re=40$.

	C_D			Nu_M		
L_d	30	40[a]	50	30	40[a]	50
Grid A (250×148)	1.758	1.7586	1.7586	12.707	12.775	12.801
Grid B (334×206)	1.765	1.766	1.766	13.163	13.165	13.165
Grid C (371×259)[a]	1.767	1.768	1.768	13.341	13.343	13.343
Grid D (476×356)	1.769	1.769	1.769	13.361	13.363	13.363

[a] Indicates the mesh size and L_d used in the study.

30D are analysed. For all cases, C_D and Nu_M remained almost unchanged with meagre variation, therefore, 21D domain height is chosen. For the sake of brevity, these details are not presented here.

It is a well-established fact that at low values of Darcy number, the porous body mimic impermeable body characteristics in terms of flow and heat transfer. Also, no literature is available for higher Pr fluids with porous bluff body. Hence, the current solver is verified at $Da = 10^{-6}$ with literature on solid square cylinder viz., Sharma and Eswaran [23] for $Pr = 0.71$ and Dhiman et al. [2] for $Pr = 1, 10$ and 100. Satisfactory confidence with the numerical results of these studies is obtained, with a maximum error of 2.4%. Current solver's feasibility for modeling porous media condition is further validated with at an intermediate value of Darcy number, $Da = 10^{-3}$ for $Pr = 0.71$. Both, coefficient of lift and mean Nusselt number showed good agreement with the numerical results presented by Dhinakaran and Ponmozhi [18], with a maximum error of less than 4%, facilitating confidence to proceed ahead with the problem in hand. Details of code validation are shown in Figs. 3 and 4.

5. Results and discussions

5.1. Parameters used in the study

Extensive 2-D numerical computations are carried out for evaluating the influence of Pr and Da on the heat transfer characteristics of the uniformly heated porous square cylinder for following range of parameters:

- Reynolds number, $Re = 1, 5$ and 10—40 in steps of 10.
- Darcy number, $Da = 10^{-6}, 10^{-4}, 10^{-3}$ and 10^{-2}.
- Porosity, ϵ = 0.629, 0.923, 0.977 and 0.997 (calculated using Carman-Kozeny relation as mentioned in Eq. (10)).
- Prandtl number, Pr = 0.71, 1, 2, 5, 10, 20, 50 and 100.

Before proceeding with an extensive discussion on results, an insight on the basic flow features around and through a porous square cylinder for the Reynolds number regime considered in the present study is provided, and the same can be visualised through Fig. 5. When the fluid flows across a porous

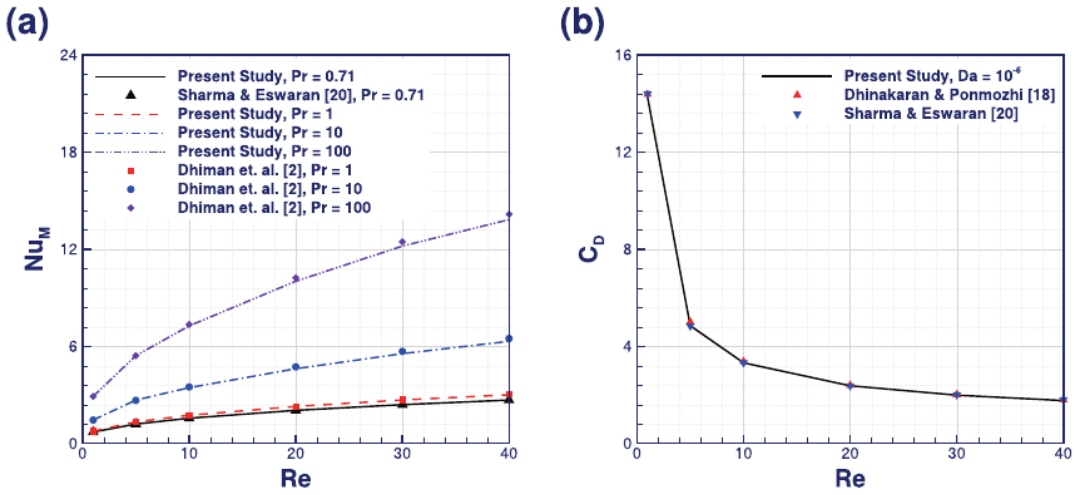

Fig. 3. Comparison of the (a) calculated mean Nusselt number, Nu_M and (b) calculated coefficient of drag at Darcy number, $Da = 10^{-6}$ (near-solid case) with the literature for different values of Reynolds number, Re and Prandtl number, Pr.

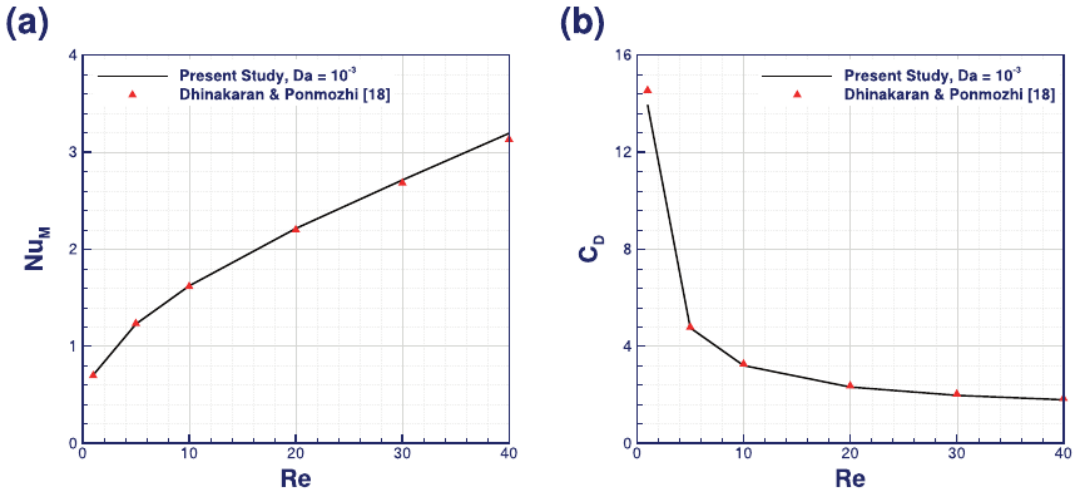

Fig. 4. Comparison of the (a) calculated mean Nusselt number, Nu_M and (b) calculated coefficient of drag (C_D) with the literature at $Da = 10^{-3}$ and Prandtl number, $Pr = 0.71$, for different values of Reynolds number, Re.

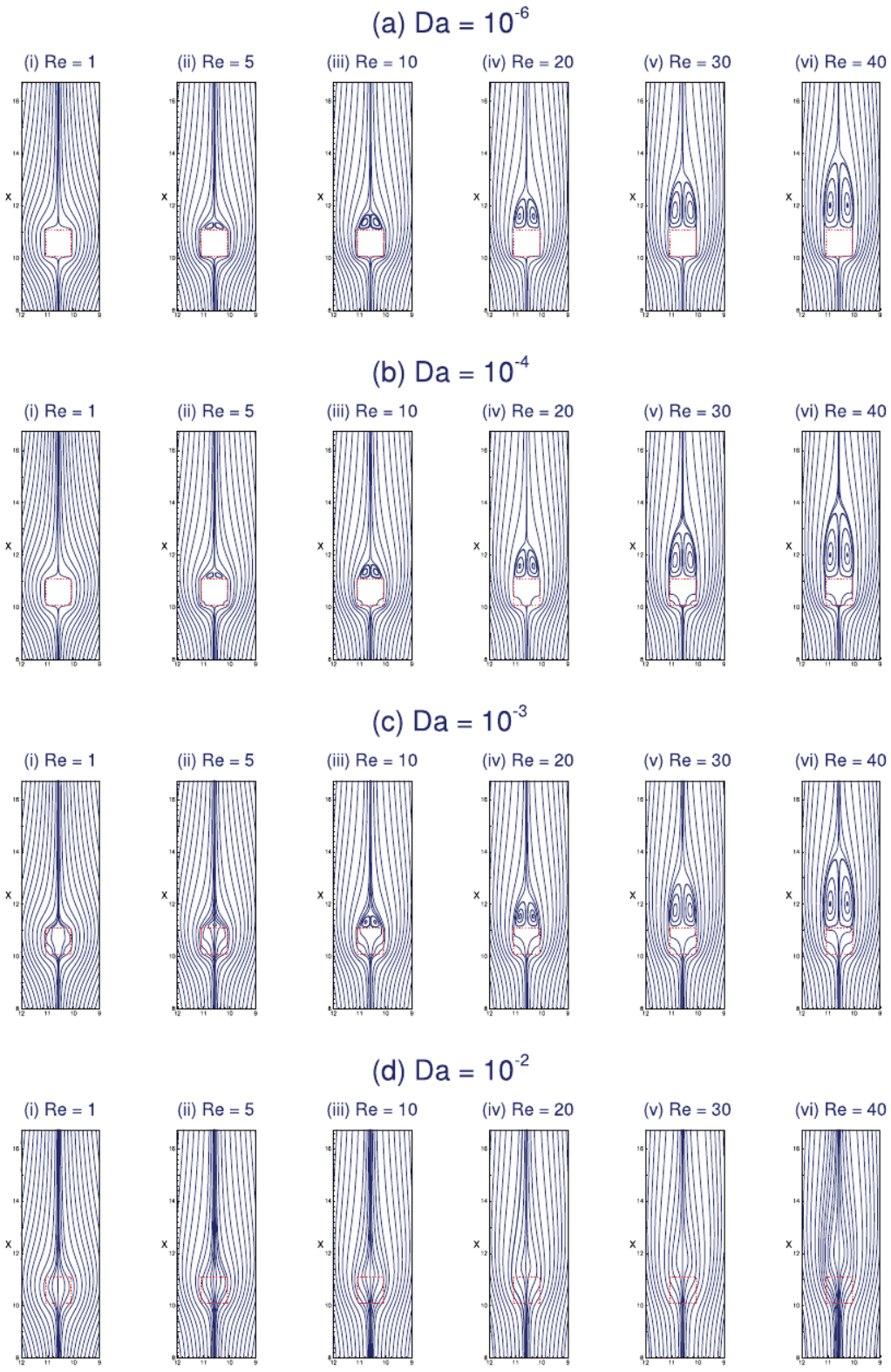

Fig. 5. Streamline contours across the porous cylinder at different values of Darcy number, $Da = 10^{-6} - 10^{-2}$ and Reynolds number, $Re = 1$—40 for a given value of Prandtl number.

square cylinder, at lower values of Darcy number e.g., at $Da = 10^{-6}$, almost no fluid enters through the porous cylinder. Hence, fluid flow pattern around the cylinder seems to be very close to that of a solid cylinder, at such low values of permeability levels. At lower Re values (< 5), the streamlines are seen to stick to the entire surface of porous cylinder. First flow separation occurs at $Re = 5$, wherein two standing wakes are seen behind the porous square cylinder. The size of this recirculation region is witnessed to increase with Reynolds number, as shown through Fig. 5(i)–(vi), due to increase in momentum of the fluid. As permeability is increased above 10^{-6} ($Da \geqslant 10^{-6}$), more amount of fluid enters through the cylinder, which results is decrement wake length behind the porous cylinder, as seen in Fig. 5(a)–(d). However, at $Da = 10^{-3}$, in contradiction to the stated understanding, a slight increase in wake length is seen inspite of higher amount of fluid flowing through the cylinder i.e., reduced resistance to the fluid flow. At lower Re ($\leqslant 10$), recirculation region shrinks and lesser wake length is noticed, which aggravates only after $Re \geqslant 20$. This jump phenomenon in flow behaviour is well-known to the literature [18] and it would be interesting to look whether it has any influence on the heat transfer from the porous square cylinder, which is discussed in the section to follow. At higher Da ($Da > 10^{-3}$), almost all the fluid flows through the cylinder, showing very less or no deflection in streamline contours in the square porous zone. This suggests that at higher permeability levels, the cylinder exerts very less or no resistance on the surround fluid, exhibiting complete suppression of recirculation region. In this study, as forced convection heat transfer is focussed on, there is no effect of Pr variation on flow characteristics. Hence, the results obtained from the numerical experiments for heat transfer are detailed, both qualitatively and quantitatively, in the sections to follow.

5.2. Isotherm contours

A qualitative representation of the thermal results is given in terms of isotherm contours in Fig. 6 for Pr = 1, 10 and 100 and Da = 10^{-6} - 10^{-2}. The right half of the plot represents $Re = 5$, while the other half represents $Re = 40$. Visual inspection of the contours reveal that by increasing Re, the flow momentum increases, decreasing the thermal boundary layer thickness. The plume is seen to advance around the cylinder, while at downstream it clings towards the symmetry line. When Pr is increased, the momentum diffusivity increases, causing the thermal boundary layer to shrink. Accordingly, the plume is witnessed to embrace the porous square cylinder tighter. Darcy number, which is the non-dimensional measure of permeability, dictates the amount of fluid entering through the cylinder. At higher Da values, more fluid flows through the heated porous cylinder, carrying away larger amount of heat from it. This can be seen from Fig. 6(i)–(iv), wherein by increasing Da, the thermal plume is witnessed stretching away from top and bottom faces of the cylinder and downstream, while becoming almost flat on the front face. The overall influence of these phenomena would be an increment in thermal gradient on the front face of the cylinder and reduction of the same for top, bottom and rear faces of the cylinder.

At lower values of Re and Pr, viscous forces are dominant, suggesting that thermal diffusivity is weakly developing. Hence, even after increasing Da up to 10^{-2}, negligible spreading of isotherms is evident, suggesting lesser increases in thermal dissipation of heat from the heated cylinder. However, as Pr is increased, momentum diffusivity compels the plume to shrink towards symmetry line and at higher Da and Pr values, the plume almost separates from rear face of the cylinder and sticks flat to the front face, indicating that most of the heat transfer occurs from the front face of the cylinder i.e. acute rise in thermal gradient at this face.

At higher values of Re, inertial forces are dominant and they pull the plume towards porous cylinder surfaces, for lower Da values. The intensity of isotherms crowding at front, top and bottom faces of the cylinder increases considerably along with twisting of these temperature profiles behind the rear face. It should be mentioned that the twisting increases with both Re and Pr and its length matches with the recirculation region behind the cylinder. As permeability of the cylinder is raised above the impermeable case, in accordance with convention, length of recirculation region should decrease due to fluid entrainment inside the cylinder. However, a jump in the values of all flow parameters at $Da = 10^{-3}$ has already been reported in the literature [18]. Following this trend, the curl length of isotherms should have been more at $Da = 10^{-3}$ in comparison to $Da = 10^{-4}$. Surprisingly, rather obviously, this is not the case, due to dominance of thermal diffusion at such values of permeability, as shown in Fig. 7. The left side of Fig. 7 represents the streamline contours and the right side shows the isotherm contours across the heated porous cylinder. As more fluid enters the heated porous cylinder at $Da = 10^{-3}$ compared to $Da = 10^{-4}$, large amount of heat is carried away from the front, top and bottom faces of the cylinder, causing the plume to separate from the rear face and elongate along the symmetry line downstream. This phenomenon becomes more severe at even higher Darcy number i.e., $Da = 10^{-2}$, wherein the plume is seen to move away from the symmetry line, as shown in Fig. 6c(iv). In order to verify that whether or not the plume meets at symmetry line, large downstream lengths of 100D and 150D were tested for and it was confirmed that even at such high values of Da and Pr the thermal plume does not meet the symmetry line at all or in other words it may touch back the symmetry line at infinity. The consequence of this being that almost no heat transfer occurs from rear face of the porous cylinder due to low value of thermal gradient on the face, indicating that most of the exchange of heat transfer must have occurred at front, top and bottom faces.

In order to give further insight on 'twisting' of isotherms behind the porous square cylinder, Fig. 8 is plotted. Isotherm contours at $\theta = 0.8$ and 0.94 are drawn at different values of Re (at $Pr = 100$) and Pr (at $Re = 40$) for intermediate value of $Da = 10^{-3}$. Different values of isotherm contour are taken for easy understanding of the occurring phenomenon. It has been stated earlier that as Re increases, intensity of recirculation region behind the cylinder rises, causing the isotherms' curling to augment, at lower values of Da. Also, as higher Pr fluid is chosen, isotherms start crowding around the cylinder and the contours further curl up behind the rear cylinder surface. However, this logic is defied for $Da \geqslant 10^{-3}$, wherein with rising momentum the isotherms initially curl a little (up to $Re = 10$), but then stretch out and move downstream as Re is further increased. A similar occurrence is seen to happen for Pr variation too i.e., the isotherm initially warps up to $Pr = 10$, but later it relaxes and moves downstream by elongating. At even higher Pr values ($Pr = 100$), it is seen that lower value of isotherm contour warp compared to lower Pr fluids, indicating higher gradient of temperature. The influence of permeability levels on twisting of isotherm contours across porous cylinder is shown in Fig. 8(c). As permeability is increased beyond impermeable limit i.e., $Da \geqslant 10^{-6}$, the isotherms untwist rapidly and elongate with increasing girth near the top and bottom faces of the

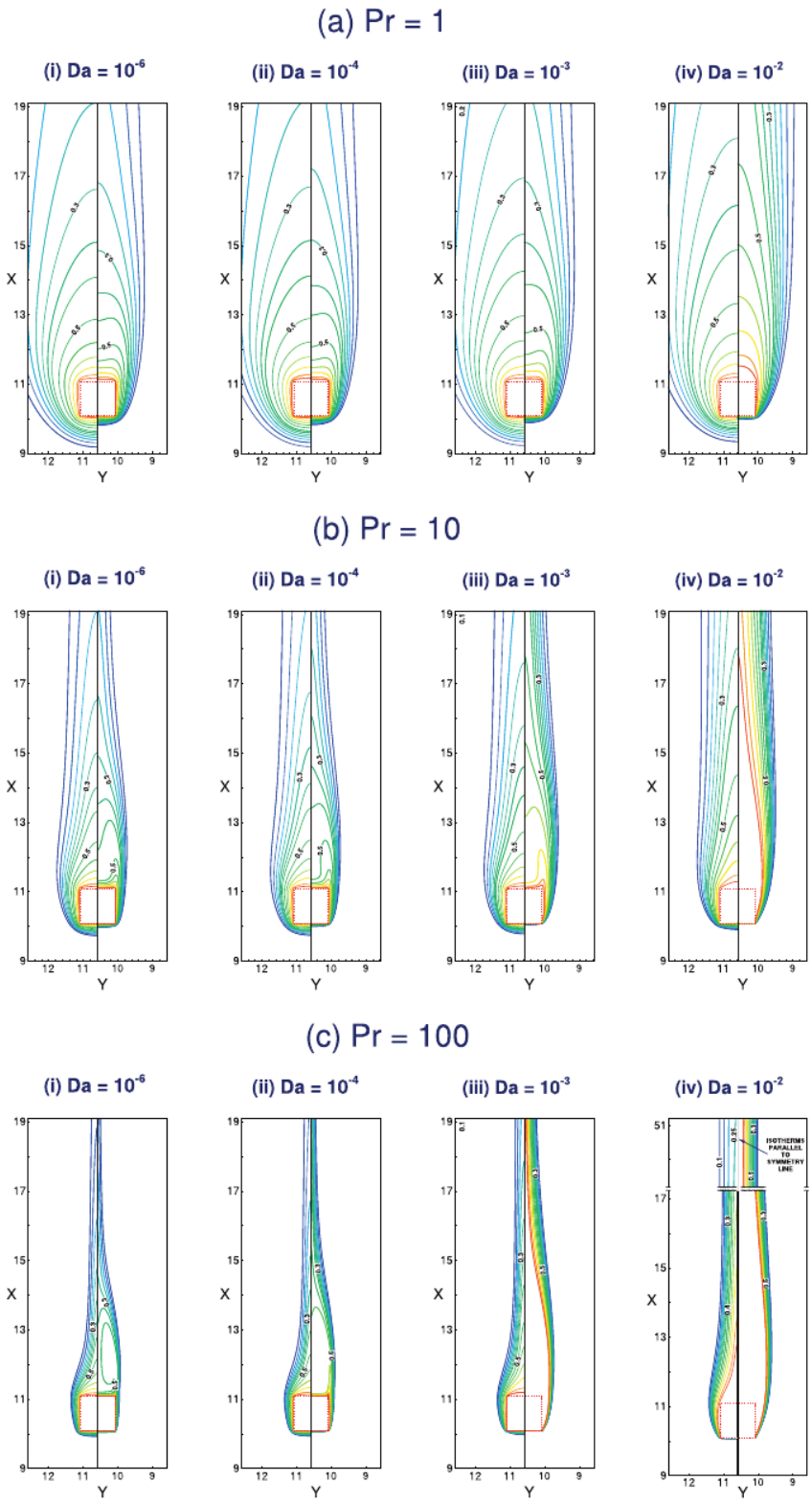

Fig. 6. Isotherm contours across the porous cylinder at different values of Prandtl number, $Pr = 1, 10$ and 100 and Darcy number, $Da = 10^{-6} - 10^{-2}$ at Reynolds number, $Re = 5$ and 40 (left side isotherm contours represent $Re = 5$ and right side isotherm contours represent $Re = 40$).

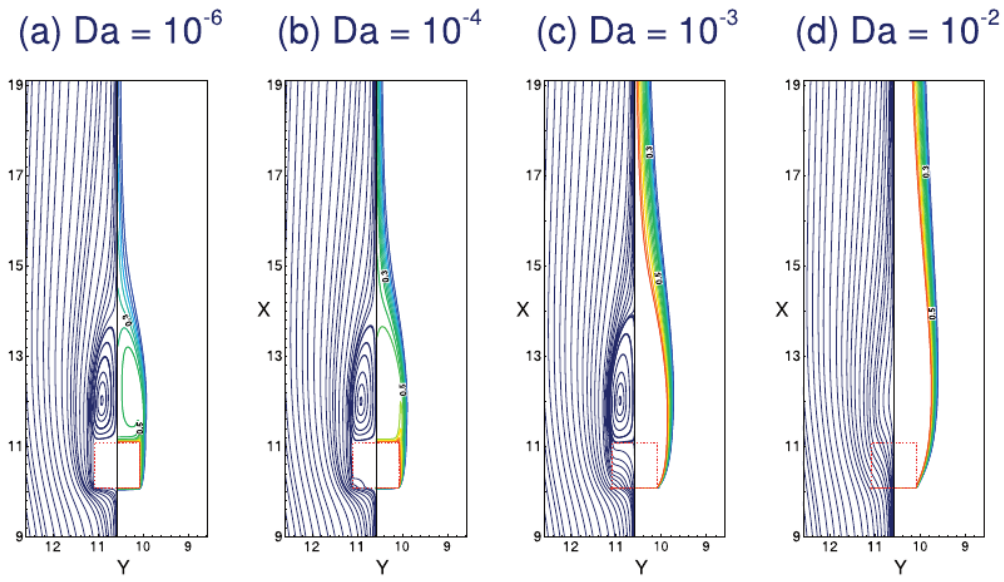

Fig. 7. Influence of jump phenomenon occurring for porous square cylinder on isotherm traits behind the cylinder at various values of Darcy number *Da* for Prandtl number, $Pr = 100$ and Reynolds number, $Re = 40$ (left side contours represent streamlines of the flow and right side contours represent isotherm profiles across the cylinder).

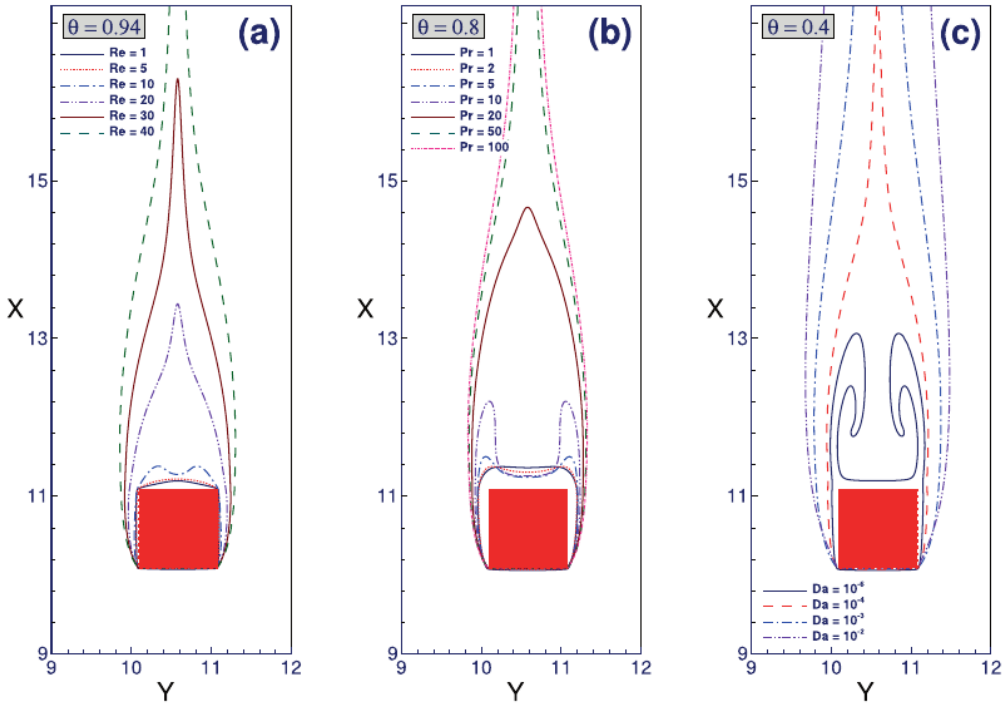

Fig. 8. Comparison of isotherm contours around and distant downstream of the porous square cylinder for (a) various Reynolds number, *Re*, at Darcy number, $Da = 10^{-3}$ and $Pr = 100$; (b) various Prandtl number, *Pr* at $Da = 10^{-3}$ and $Re = 40$; (c) various *Da* values at $Pr = 100$ and $Re = 40$.

cylinder. In order to further elucidate this phenomenon, temperature profiles are plotted at 1*D* distance normal to the rear face of the porous cylinder in the vertical direction i.e., along *Y*-axis for $Re = 40$ at various *Da* and *Pr* values, as shown in Fig. 9. It is clear that at lower *Pr* values, by increasing permeability, the isotherms untwist steadily, with higher temperature values and the curling of these 'twists' relaxes into a bell shaped dome until becoming completely flat with the cylinder temperature at $Da = 10^{-2}$. This supports the ideology of isotherms separating away from rear face and from the symmetry line at higher permeability, reducing the thermal gradient at that face. At higher *Pr* and lower *Da* values, as seen in Fig. 9 earlier, due to sharp

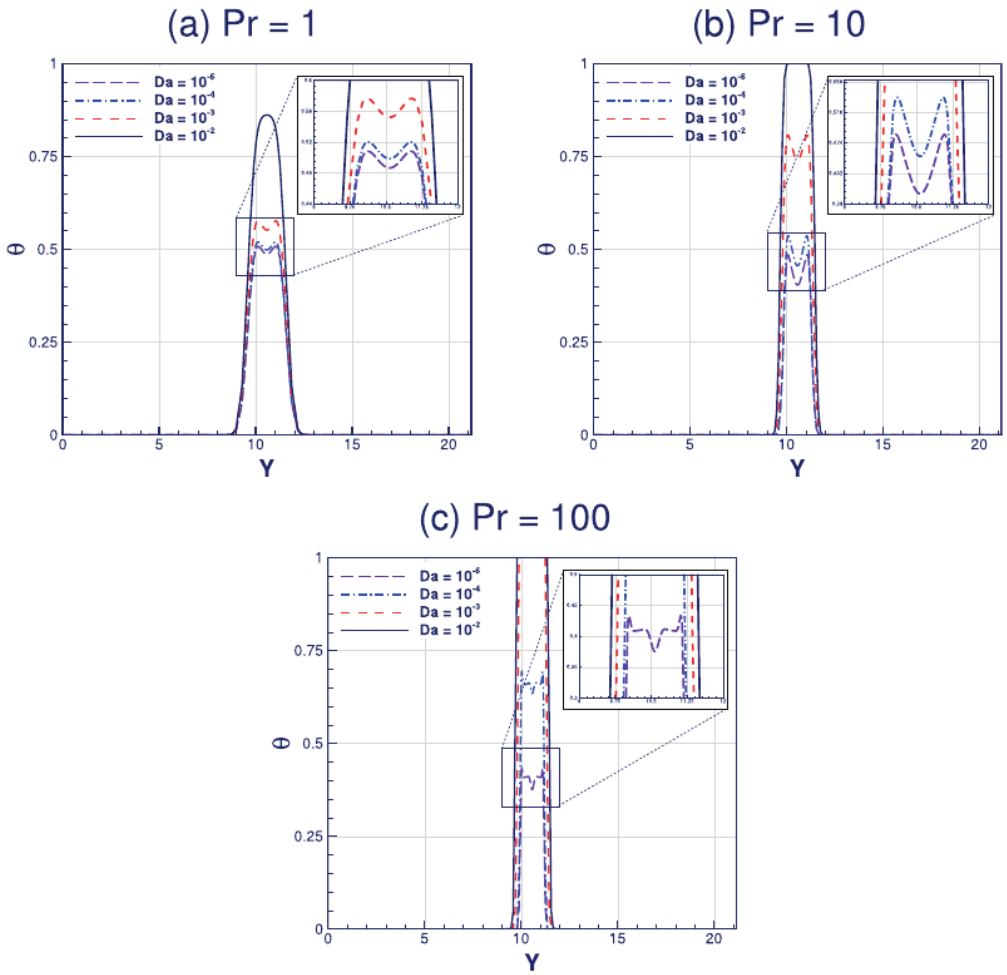

Fig. 9. Temperature distribution in the vertical direction at 1*D* distance away from rear face of the porous square cylinder for various Prandtl number, *Pr* and Darcy number, *Da* values at Reynolds number, *Re* = 40.

warping of isotherms a distinct kink is witnessed at the corners of the sine-like temperature curves. These kinks reduce as more fluid enters through the heated cylinder i.e., *Da* value is increased and they acquire higher values in temperature until reaching the far-fluid temperature.

5.3. Local Nusselt number distribution

The local Nusselt distribution over upper half of the porous square cylinder is displayed in Fig. 10 for $Pr = 1, 10$ and 100 and $Re = 1$ and 40 at various levels of permeability. In the present study, the local *Nu* distribution is defined as $-R_k \frac{\partial \theta}{\partial n}$, as constant temperature boundary condition is imposed on the heated porous cylinder surface (R_k refers to thermal conductivity ratio). It is to be mentioned that since the corners are taken as the beginning of thermal boundary layer, a spike in the value of Nusselt number at these corners is observed due to high thermal gradients normal to the surface of porous body. Because of this singularity nature at the corners, special emphasis was laid on the grid size at the corners of the porous obstacle, as *Nu* value is reported to progressively decrease with coarser grids. For the last two fine grids chosen in the grid independence (Table 1), an error of less than 5% was found. Although, this may suggest that the corner values are strongly dependent on grid size, it should be noted that the overall surface average Nusselt number varies negligibly with the values of these vanishingly little heat dissipation area corner points. The chosen grid size is fine enough to deliver global thermal results that are independent of grid structure.

It is evident that, as seen earlier in isotherm contours, the difference between *Nu* for front and rear face of the cylinder increases considerably with rising permeability levels. Most of the heat transfer must occur from the front face of the cylinder for higher Darcy number, as the same is witnessed through Fig. 10(ii) for all *Pr* values. Importantly, the difference in *Nu* between each permeability level increases with *Pr* and this effect is prominent for $Da = 10^{-3} - 10^{-2}$. Also, every face seems to have a local minimum value of *Nu*, whose position change with Darcy number considerably. For rear face, this point moves towards top face, due to changes in the functioning of heat transfer by the stronger vortices. Higher entrainment of fluid through the cylinder further causes the local minimum point move towards front face of the cylinder for top and bottom faces of the cylinder. Noticeably, at higher Re, Da and *Pr* values, a stalling in the growth of *Nu* is seen, wherein the variation in local *Nu* is almost flat over the front face of the cylinder along with a sharp kink in the curve at the corner.

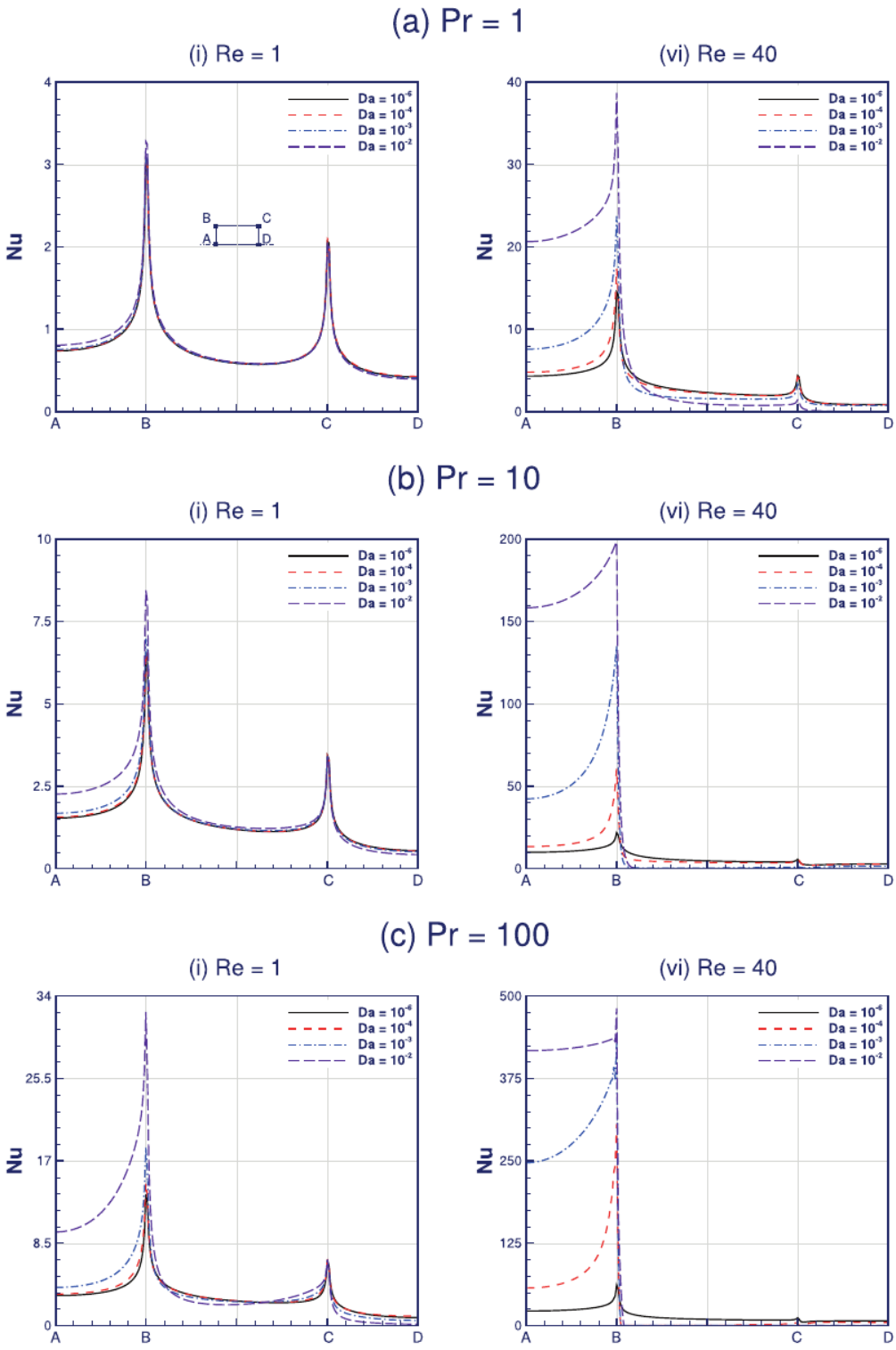

Fig. 10. Variation of local Nusselt number over the surface of porous square cylinder for Reynolds number, *Re* = 1 and 40 and Prandtl number, *Pr* = 1, 10 and 100 at different values of Darcy number, *Da*.

5.4. Heat transfer augmentation for different faces

In order to further provide a vivid picture of the above variation, enhancement ratio of Nusselt number is plotted for difference faces of the porous square cylinder, as shown in Figs. 11–13. A three point backward interpolation procedure is implemented on the local *Nu* variation for a particular face of the cylinder and surface average values are obtained. Further,

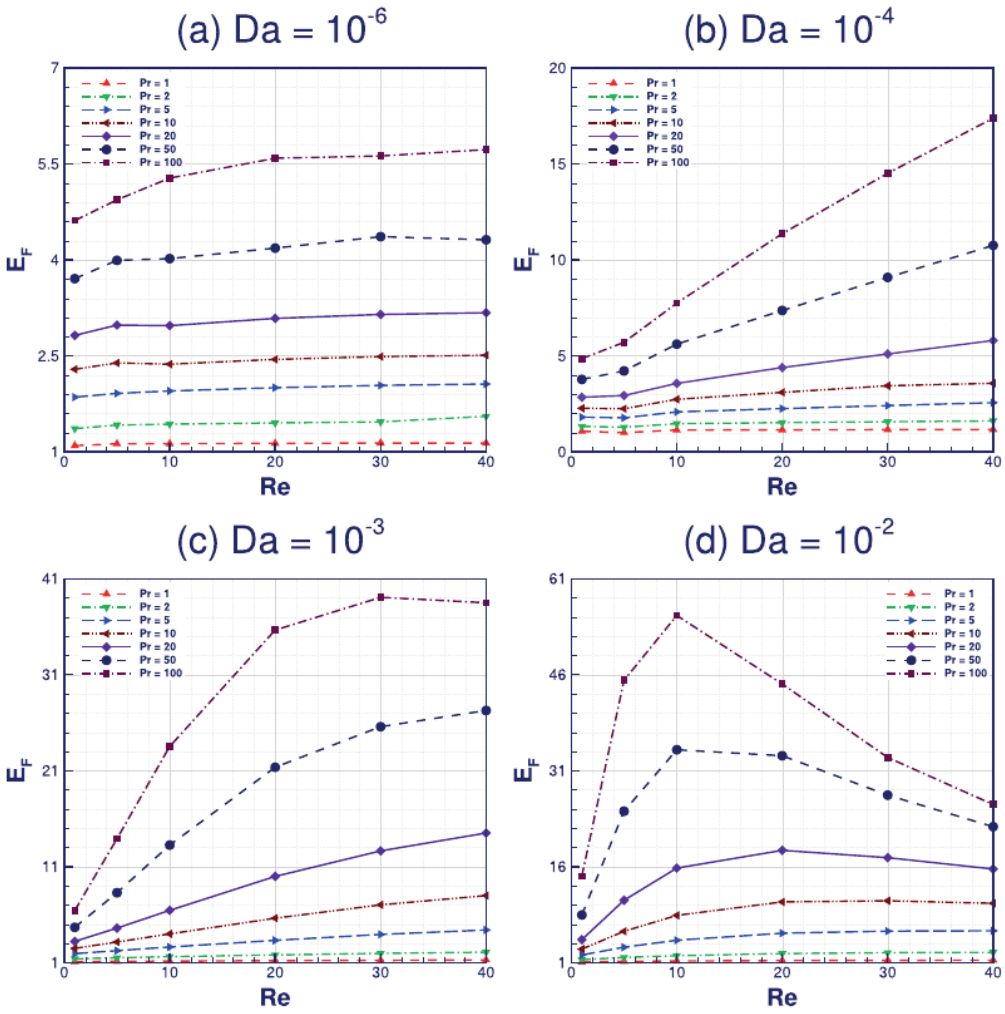

Fig. 11. Variation of enhancement ratio of Nusselt number for the frontal surface of porous square cylinder at various Reynolds number, *Re*, Prandtl number, *Pr*, and Darcy number, *Da* values.

the enhancement ratio for a particular face is calculated by dividing the surface average *Nu* at a given *Pr* value with that at $Pr = 0.71$, for a particular value of Reynolds number and Darcy number.

For the front face, as shown in Fig. 11, at $Da = 10^{-6}$, the rise in enhancement ratio (E_F) values with *Pr* is obvious due to thinning of thermal boundary layer at higher *Pr* values. However, for a given Prandtl number, increasing flow across cylinder provides meagre or no rise in enhancement ratio, suggesting dissipation of maximum heat away from the cylinder. However, as permeability level is increased from $Da = 10^{-6}$ to $Da = 10^{-4}$, significant variation in E_F trends are visible in Fig. 11(b), as the amount of fluid flow through the heated porous body augments. For instance, at $Re = 40$ and $Pr = 100$, enhancement ratio jumps from 5.725 to 17.384 when Darcy number changes from $Da = 10^{-6}$ to $Da = 10^{-4}$. The hot front face of cylinder, which receives undisturbed flow, exhibits rise in enhancement ratio, with *Re* and *Pr*. At even higher permeability levels i.e., $Da = 10^{-3}$, as the flow through front faces increases almost to through flow condition with lesser deviation, the thermal boundary layer at this face thins out considerably. This results is stunting in the growth in E_F at higher *Pr* and *Re* values. The decline in this trend becomes severe at even higher *Da* values e.g., $Da = 10^{-2}$, as the through flow condition exists and the hot surface is highly permeable, providing least resistance to incoming flow. At $Pr = 100$ and $Da = 10^{-3}$, the enhancement ratio reduces from 39.058 to 38.490 when the Reynolds number is increased from $Re = 30$ to $Re = 40$. Further, at $Pr = 100$ and $Da = 10^{-2}$, the enhancement ratio declines from 33.063 to 25.716. Maximum heat dissipation seems to occur at lower *Re* and *Pr* values at this permeability level, and although surface average *Nu* increases, the enhancement ratio decreases at higher *Re* and *Pr* values.

Since, the flow remains steady for entire range of *Re* considered, heat transfer traits shown by top and bottom faces of the porous cylinder remains identical. Enhancement ratio fashion for top and/or bottom surfaces (E_T or E_B) are displayed in Fig. 12. As discussed above, the front surface receives undisturbed flow, but the top and bottom faces do not. At lower *Re* values ($Re < 5$), before flow separation occurs, the thermal boundary layer is thick and is almost evenly spread across the porous cylinder, as shown in Figs. 6 (a–c)(i). Therefore, E_T is witnessed to rise with *Re* and *Pr* at lower values of *Da*, as the thinning of thermal boundary layer i.e. increase in thermal gradient at the face is meagre. The rise in local Nusselt number augments from 1.074% to 4.449 by changing Prandtl

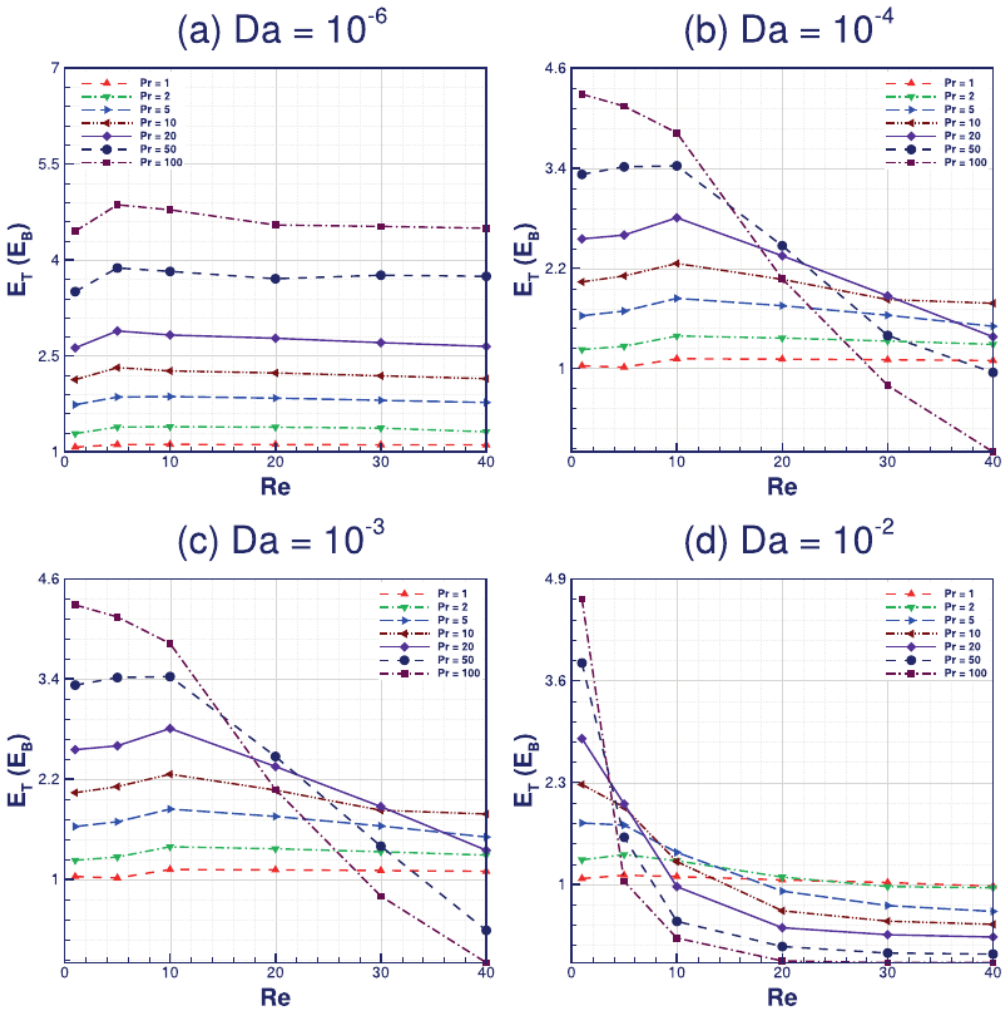

Fig. 12. Variation of enhancement ratio of Nusselt number for top and bottom surfaces of porous square cylinder at various Reynolds number, *Re*, Prandtl number, *Pr*, and Darcy number, *Da* values.

number from *Pr* = 1 to *Pr* = 100, at *Re* = 1 and $Da = 10^{-6}$. When momentum of the fluid increases beyond separation point, the thermal gradient at these faces decline due to bulging of thermal boundary layer. Also, the fluid penetrating front face diverts due to porous resistance and moves towards top and bottom faces. Since, this fluid has already exchanged heat with front face, thermal interaction between such a fluid and top and bottom faces should be less. Overall, a drop in the surface average *Nu* value, inturn enhancement ratio is reported at higher *Pr*, *Da* and *Re* values. Such decline in enhancement ratio also occurs due to thickening of thermal boundary layer at higher *Da* values, inspite of extreme *Re* and *Pr* conditions, indicating the tendency of porous surface to attain far-fluid temperature. The enhancement ratio value diminishes from 4.496 to 0 when Darcy number increases from $Da = 10^{-6}$ to $Da \geqslant 10^{-4}$, at $Re = 40$ and $Pr = 100$.

Mixed trends in enhancement ratio is evident for the rear face (E_R) of porous square cylinder, as displayed in Fig. 13. For lower permeability level ($Da = 10^{-6}$), E_R exhibits a linear trend with *Re*, *Pr* and *Da*. At higher values of *Re*, E_F appears to have reached saturation, but E_R increases linearly and is found to be higher than E_F and E_T (or E_B). It is well-known that with momentum, the recirculation region increases behind the porous cylinder, although surface average *Nu* is less than the front face, E_R is found to be higher than E_F at higher *Re*, *Pr* and *Da* values. At $Pr = 100$ and $Da = 10^{-6}$, the difference is quite apparent as E_R = 6.771, while E_F = 5.725. This linear fashion stays at $Da = 10^{-4}$, but a reduction in E_R values is clear. Comparatively higher entrainment of fluid into the cylinder reduces recirculation region, which results in such decrement in E_R. At $Da = 10^{-3}$, a jump in flow parameters has been reported in the literature and is confirmed in the present study (discussed in Section 5.2). Although this jump phenomenon does not hamper the isotherm contours, the enhancement ratio exhibits an anomalous trend up to $Pr = 20$. Wherein, initially E_R decreases up to $Re = 20$ and then increases monotonously. At even higher *Pr* values, this trend succumbs and a linear decrease up to zero is reported. Such decrement is inline with the understanding given for E_F and E_T variation that most of the heat dissipation must have occurred at front, top and bottom faces, which causes E_R to reduce. Similar occurrence is seen at $Da = 10^{-2}$, wherein the through-flow-like condition exists. Therefore, the fluid that reaches rear face post-penetration is almost heated to cylinder temperature, which causes a decreasing trend in E_R and it becomes zero even for higher *Re* and *Pr* values.

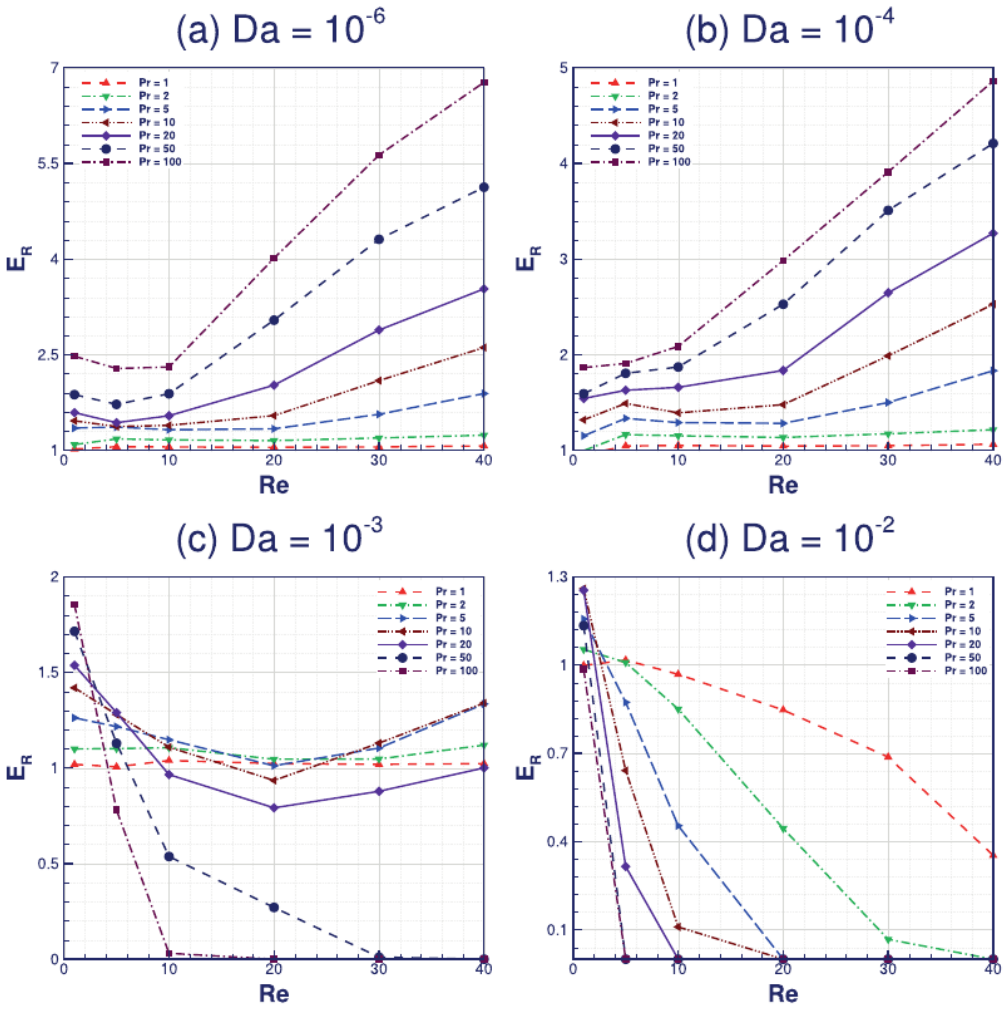

Fig. 13. Variation of enhancement ratio of Nusselt number for the rear surface of porous square cylinder at various Reynolds number, *Re*, Prandtl number, *Pr*, and Darcy number, *Da* values.

In summary, higher-*Pr* fluids causes significant enhancement in heat transfer at frontal face of the porous cylinder, followed by top and bottom faces. The role of rear face in enhancement ratio appears to be meagre except for at lower *Da* values, wherein E_R is found to be higher than E_F and E_T at higher *Re* and *Pr* values. Enhancement ratio of rear face further decreases, followed by complete suppression as *Da* is increased.

5.5. Mean Nusselt number variation

A cumulative effect of the above variation of enhancement ratio of surface *Nu* values can be quantitatively analysed through mean Nusselt number plots, displayed in Fig. 14 and enhancement ratio (as calculated above) values given in Tables 3 and 4. Even though contribution of rear, top and bottom faces of the cylinder in overall heat transfer diminishes at higher *Pr* and *Da* values, the front surface makes it up for the loss and an steep rise in Nu_M is clear with *Pr*, *Da* and *Re*. Arguably, at the peak values of parameters taken into this study, as seen before, the increment in Nu_M is seen to stall. At $Re = 1$, the enhancement ratio value for $Pr = 1$ and $Da = 10^{-6}$ is 7.184, and this value increases to 47.956 for $Pr = 100$ and $Da = 10^{-2}$. Considering the stalling phenomenon, at $Re = 40$, this increment in enhancement ratio increases from 11.778 to 15.455 only. The maximum enhancement ratio point does not lie at the extremities of the parameter range, but at $Da = 10^{-3}$ and $Pr = 50$ for $Re = 40$. A least square curve is fitted with correlation coefficient maintained around 1 and maximum error limited within 13%. Correlations are built for Nu_M at $Pr = 1$, 10 and 100 and different Darcy number values in terms of *Re* and are listed in Table 2. It is seen that the power of *Re* decreases instead of increasing at $Pr = 100$ and $Da = 10^{-2}$, which supports stalling concept. Elsewhere, a direct proportion between Nu_M and simulation parameters is evident. Importantly, the overall increment in heat transfer rate is still high, wherein a 668.78% rise is reported for $Da = 10^{-2}$ with respect to $Da = 10^{-6}$ at $Pr = 100$ and $Re = 40$, which is 124.63% for $Da = 10^{-2}$ with respect to $Da = 10^{-6}$ at $Pr = 1$ and $Re = 40$.

5.6. Validity of Forchheimer Term

It is well-known that for flow in porous media, as the Reynolds number (*Re*) increases (exceeds approximately $Re = 10$),

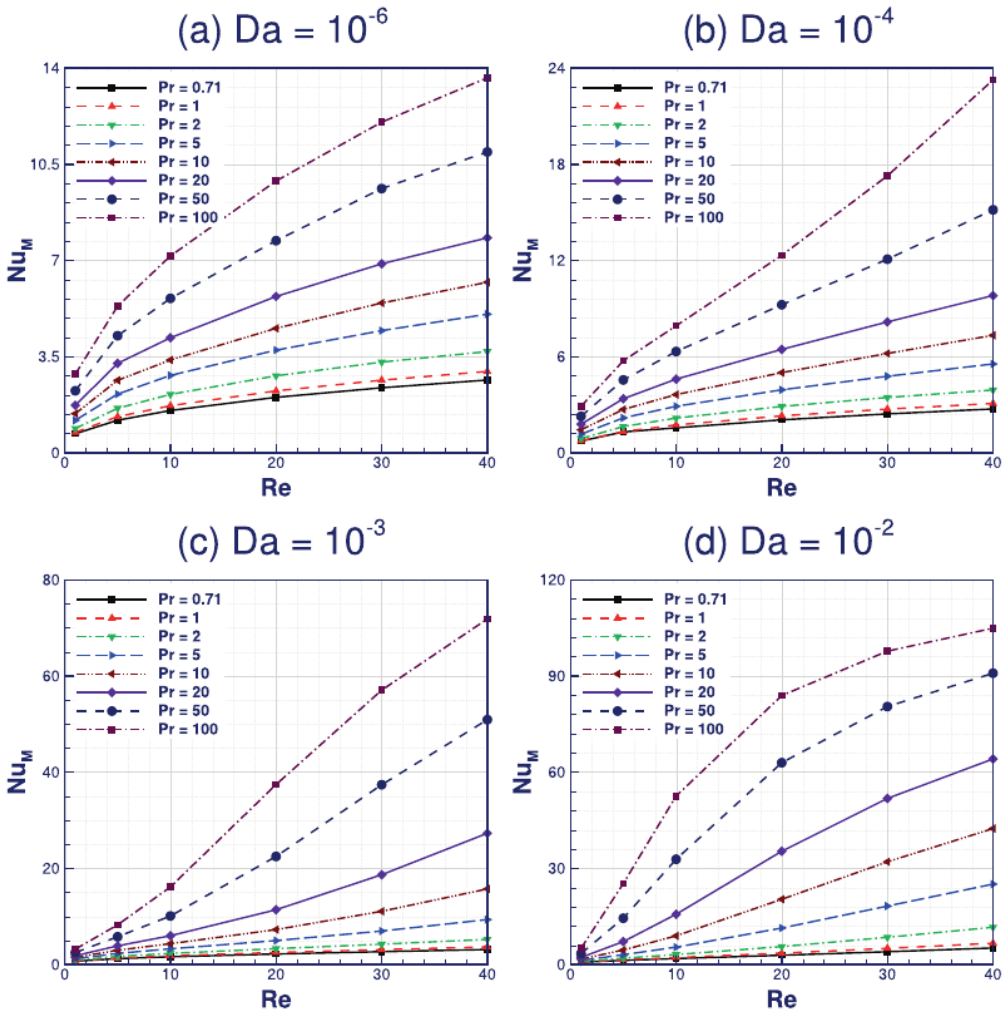

Fig. 14. Variation of mean Nusselt number for the porous square cylinder at various Reynolds number, *Re*, Prandtl number, *Pr*, and Darcy number, *Da* values.

Table 2
Correlations obtained for Nu_M by fitting least square curves for Prandtl number, Pr = 1, 10 and 100 at various values of Darcy number, *Da* in terms of Reynolds number, *Re*.

	$Pr = 1$	$Pr = 10$	$Pr = 100$
$Da = 10^{-6}$	$0.714 \times Re^{0.384}$	$1.336 \times Re^{0.413}$	$2.619 \times Re^{0.446}$
$Da = 10^{-4}$	$0.706 \times Re^{0.397}$	$1.244 \times Re^{0.475}$	$1.525 \times Re^{0.726}$
$Da = 10^{-3}$	$0.634 \times Re^{0.469}$	$0.513 \times Re^{0.917}$	$1.791 \times Re^{1.006}$
$Da = 10^{-2}$	$0.389 \times Re^{0.761}$	$0.809 \times Re^{1.076}$	$7.427 \times Re^{0.754}$

inertial effects become significant. Forchheimer term accounts for the non-linear trend of pressure drop with flow velocity. From the simulations results, such trends are confirmed, wherein some changes in flow and heat transfer traits are visible after $Re = 10$, as shown in Tables 5 and 6. But the deviation in flow and heat transfer parameters are seen to be meagre. Hence, it is clear that in the present flow regime i.e., Re = 1–40, difference in flow and heat transfer traits due to presence of the Forchheimer term is nominal and can be overlooked. However, it should be also noted that as the Reynolds number increases, role of Forchheimer term becomes severe. For instance, at $Re = 100$ and $Da = 10^{-2}$, the percentage deviation in coefficient of drag can increase up to 15.248%, on the basis of a simulation data. This point provides an impetus for further study on the role of Forchheimer term in unsteady flow regime.

Table 3
Enhancement in mean Nusselt number (Nu_M) calculated with respect to Prandtl number, $Pr = 0.71$ at various Pr values for Reynolds number, $Re = 1$.

	$Pr = 1$	$Pr = 2$	$Pr = 5$	$Pr = 10$	$Pr = 20$	$Pr = 50$	$Pr = 100$
$Da = 10^{-6}$	7.184	18.633	33.446	20.660	21.263	30.787	26.681
$Da = 10^{-4}$	2.729	17.795	31.116	23.560	24.148	27.578	27.592
$Da = 10^{-4}$	7.615	20.294	32.075	24.454	23.835	35.823	28.181
$Da = 10^{-2}$	7.273	22.295	37.100	30.793	32.283	53.888	47.956

Table 4
Enhancement in mean Nusselt number (Nu_M) calculated with respect to Prandtl number, $Pr = 0.71$ at various Pr values for Reynolds number, $Re = 40$.

	$Pr = 1$	$Pr = 2$	$Pr = 5$	$Pr = 10$	$Pr = 20$	$Pr = 50$	$Pr = 100$
$Da = 10^{-6}$	11.778	24.417	36.971	22.969	26.092	39.941	24.642
$Da = 10^{-4}$	12.578	27.347	41.367	32.239	33.847	54.480	53.484
$Da = 10^{-4}$	17.072	42.900	78.655	68.232	73.550	86.540	41.131
$Da = 10^{-2}$	28.920	74.771	115.812	69.082	51.198	41.694	15.455

Table 5
Comparison of coefficient of drag (C_D) and mean Nusselt number (Nu_M) values at $Da = 10^{-6}$ for Darcy-Brinkman-Forchheimer model (D-B-F) and Darcy-Brinkman Model (D-B).

	C_D			Nu_M		
Re	D-B-F	D-B	% Deviation	D-B-F	D-B	% Deviation
1	14.243	14.243	0.000	2.863	2.873	−0.349
5	4.850	4.850	0.000	5.338	5.353	−0.281
10	3.211	3.211	0.000	7.163	7.174	−0.154
20	2.376	2.376	0.000	9.892	9.900	−0.081
30	1.989	1.989	0.000	12.033	12.031	0.017
40	1.768	1.768	0.000	13.647	13.621	0.191

Table 6
Comparison of coefficient of drag (C_D) and mean Nusselt number (Nu_M) values at $Da = 10^{-2}$ for Darcy-Brinkman-Forchheimer model (D-B-F) and Darcy-Brinkman Model (D-B).

	C_D			Nu_M		
Re	D-B-F	D-B	% Deviation	D-B-F	D-B	% Deviation
1	12.448	12.449	−0.008	5.066	5.073	−0.138
5	4.198	4.199	−0.024	25.278	25.364	−0.340
10	2.908	2.909	−0.034	52.555	52.862	−0.584
20	2.164	2.146	0.832	83.906	84.570	−0.791
30	1.885	1.856	1.538	97.751	98.786	−1.059
40	1.732	1.688	2.540	104.915	106.075	−1.106

6. Conclusions

A numerical study on the effects of Prandtl number on forced convection heat transfer from a square cylinder is presented for $Pr = 0.71$—$100, Re = 1$—40 and $Da = 10^{-6} - 10^{-2}$. The generic buoyantBoussinesqPimpleFoam solver of OpenFOAM 5.0 is modified with the extended Darcy-Brinkman-Forchheimer model and the porosity term is included in the governing equations to account for the superficial speed of flow in the heated porous region. The isotherm contours cling around the cylinder with increasing Pr at low values of Da and for $Da \geqslant 10^{-3}$ they stick more to front face of the cylinder, while moving away from top, bottom and rear faces of the porous cylinder. The effect of which is further emphasised through local Nusselt number and enhancement ratio plots, wherein a steep rise and stalling in Nu is seen for front face and a steady decline is encountered for the rest of the faces, with increasing Re, Pr and Da. However, a mammoth rise in overall heat transfer from the porous cylinder is reported. The twisting and untwisting of isotherms behind the porous cylinder and their implications on the thermal gradient, inturn Nu for different faces are detailed. Further, an insight is given on the influence of jump phenomenon, that occurs into flow characteristics of porous square cylinder with increasing Da, on heat transfer. It is seen that the heat transfer pattern is undisturbed by the 'jump'. However, surface Nusselt number values are influenced by this anomalous feature for rear surface of the porous cylinder. Finally, a few correlations were provided in terms of Reynolds number for different Pr and Da values and it is seen that the enhancement in thermal dissipation stalls at higher Pr and Da values. Nevertheless, a ginormous augmentation in mean Nusselt number from 124.63% to 668.78% is disclosed at $Da = 10^{-2}$ and $Re = 40$ with respect to $Da = 10^{-6}$ for $Pr = 1$ and $Pr = 100$, respectively. Insight is also provided on the role of Forchheimer term in modelling flow and heat transfer from porous square cylinder in steady flow regime. It is seen that the inertial source term plays a meagre role in accounting porous resistance and hence, can be overlooked in the Reynolds number range of $1 \leqslant Re \leqslant 40$.

Conflict of interest

None.

Acknowledgement

One of the authors, S. Dhinakaran, gratefully acknowledges the financial aid received from Council of Scientific & Industrial Research (CSIR), Government of India through a project grant (Project Reference No. 22(0642)/13/EMR-II) for carrying out this work. The authors are highly obliged to the reviewers for their insightful comments and suggestions.

References

[1] A. Dhiman, R. Chhabra, V. Eswaran, Flow and heat transfer across a confined square cylinder in the steady flow regime: effect of Peclet number, Int. J. Heat Mass Transf. 48 (2005) 4598–4614.
[2] A. Dhiman, R. Chhabra, A. Sharma, V. Eswaran, Effects of reynolds and Prandtl numbers on heat transfer across a square cylinder in the steady flow regime, Numer. Heat Transf., Part A: Appl. 49 (2006) 717–731.
[3] R.P. Bharti, R. Chhabra, V. Eswaran, A numerical study of the steady forced convection heat transfer from an unconfined circular cylinder, Heat Mass Transf. 43 (2007) 639–648.
[4] A.K. Sahu, R. Chhabra, V. Eswaran, Effects of reynolds and Prandtl numbers on heat transfer from a square cylinder in the unsteady flow regime, Int. J. Heat Mass Transf. 52 (2009) 839–850.

[5] S. Sarkar, A. Dalal, G. Biswas, Unsteady wake dynamics and heat transfer in forced and mixed convection past a circular cylinder in cross flow for high Prandtl numbers, Int. J. Heat Mass Transf. 54 (2011) 3536–3551 .
[6] D. Kumar, A.K. Dhiman, Computations of incompressible fluid flow around a long square obstacle near a wall: laminar forced flow and thermal characteristics, Sādhanā 42 (2017) 941–961 .
[7] Q. Chen, X. Zhang, J. Zhang, Effects of Reynolds and Prandtl numbers on heat transfer around a circular cylinder by the simplified thermal lattice boltzmann model, Commun. Comput. Phys. 17 (2015) 937–959 .
[8] S. Ajith Kumar, M. Mathur, A. Sameen, S. Anil Lal, Effects of Prandtl number on the laminar cross flow past a heated cylinder, Phys. Fluids 28 (2016) 113603 .
[9] J. Aboueian-Jahromi, A.H. Nezhad, A. Behzadmehr, Effects of blockage ratio and Prandtl number on steady flow and heat transfer around an inclined square cylinder, Heat Transf. Res. 46 (2015) 541–562 .
[10] A. Chandra, R. Chhabra, Flow over and forced convection heat transfer in newtonian fluids from a semi-circular cylinder, Int. J. Heat Mass Transf. 54 (2011) 225–241 .
[11] A. Gode, A.K. Sahu, R. Chhabra, Two-dimensional steady flow over a semi-circular cylinder: drag coefficient and Nusselt number, Int. J. Adv. Eng. Sci. Appl. Math. 3 (2011) 44–59 .
[12] A. Kumar, A. Dhiman, L. Baranyi, Fluid flow and heat transfer around a confined semi-circular cylinder: onset of vortex shedding and effects of reynolds and Prandtl numbers, Int. J. Heat Mass Transf. 102 (2016) 417–425 .
[13] D. Chatterjee, B. Mondal, Forced convection heat transfer from an equilateral triangular cylinder at low reynolds numbers, Heat Mass Transf. 48 (2012) 1575–1587 .
[14] P. Dey, A.K. Das, Heat transfer enhancement around a cylinder–a CFD study of effect of corner radius and Prandtl number, Int. J. Chem. React. Eng. 14 (2016) 587–597.
[15] P. Dey, A. Das, Numerical analysis and prediction of unsteady forced convection over a sharp and rounded edged square cylinder, J. Appl. Fluid Mech. 9 (2016) 1189–1199 .
[16] H.-W. Wu, R.-H. Wang, Convective heat transfer over a heated square porous cylinder in a channel, Int. J. Heat Mass Transf. 53 (2010) 1927–1937 .
[17] S.-W. Perng, H.-W. Wu, R.-H. Wang, T.-C. Jue, Unsteady convection heat transfer for a porous square cylinder varying cylinder-to-channel height ratio, Int. J. Therm. Sci. 50 (2011) 2006–2015 .
[18] S. Dhinakaran, J. Ponmozhi, Heat transfer from a permeable square cylinder to a flowing fluid, Energy Convers. Manage. 52 (2011) 2170–2182 .
[19] R. Holdich, Fundamentals of Particle Technology, Midland Information Technology and Publishing, 2002.
[20] D.A. Nield, A. Bejan, Convection in Porous Media, vol. 3, Springer, Cham, 2006.
[21] H.G. Weller, G. Tabor, H. Jasak, C. Fureby, A tensorial approach to computational continuum mechanics using object-oriented techniques, Comput. Phys. 12 (1998) 620–631 .
[22] F. Kärrholm, C. tekniska högskola, Numerical Modelling of Diesel Spray Injection, Turbulence Interaction and Combustion, Doktorsavhandlingar vid Chalmers Tekniska Högskola: Chalmers Tekniska Högskola, Chalmers University of Technology, 2008.
[23] A. Sharma, V. Eswaran, Heat and fluid flow across a square cylinder in the two-dimensional laminar flow regime, Numer. Heat Transf., Part A: Appl. 45 (2004) 247–269.